

Electronic Supplementary Material

**A New Cobalt(II)-Lithium(I) Carboxylate Complex with N,O-Donor Mono-iminoacenaphthenone
Ligand: Synthesis, Structure and Magnetic Behavior**

Dmitriy S. Yambulatov,^{*a} Stanislav A. Nikolaevskii,^{*a} Anton N. Lukoyanov,^b Maxim A. Shmelev,^a
Julia K. Voronina,^a Konstantin A. Babeshkin,^a Anna K. Matiukhina,^a Nikolay N. Efimov,^a
Mikhail A. Kiskin^a and Igor L. Eremenko^a

^aN.S. Kurnakov Institute of General and Inorganic Chemistry of the Russian Academy of Sciences,
31 Leninsky prosp., 119991 Moscow, Russian Federation.
E-mail: yambulatov@yandex.ru, sanikol@igic.ras.ru

^bRazuvaev Institute of Organometallic Chemistry of the Russian Academy of Sciences, Tropinina,
49, 603950 Nizhny Novgorod, Russian Federation

Table of Contents

1. Synthesis	S2
1.1 General remarks	S2
1.2 Synthesis of 4-MeOC ₆ H ₄ -MIAN.....	S2
1.3 Synthesis of [Co ₂ Li ₂ (Piv) ₆ (4-MeOC ₆ H ₄ -MIAN) ₂]·CH ₃ CN (1)	S2
2. NMR spectroscopy	S4
3. IR spectroscopy	S5
4. Single crystal X-ray diffraction	S6
5. Powder X-ray diffraction studies	S8
6. Magnetochemistry	S9
7. Quantum-chemical calculations	S12
8. References	S15

1. Synthesis

1.1 General remarks

All manipulations related to the synthesis of compound **1** were accomplished in inert atmosphere. Acetonitrile was dried with P₂O₅, kept on the activated molecular sieves (4 Å) and replaced to the reaction zone by vacuum condensation with liquid nitrogen just before the synthesis. Cobalt and lithium trimethylacetates were synthesized as previously reported [S1, S2]. After isolation from the solution dry sample of **1** is stable at ambient conditions. In solution it tends to oxidation, that's why inert atmosphere should be applied during the synthesis. The initial ligand 4-MeOC₆H₄-MIAN was synthesized according to the modified procedure described in the work [S3] - the addition of acetic acid and recrystallization from acetone increased the product yield from 60 to 86 percent.

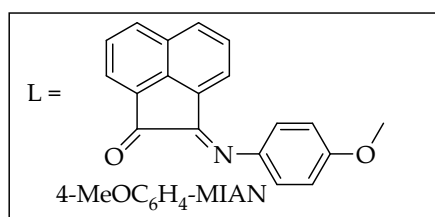
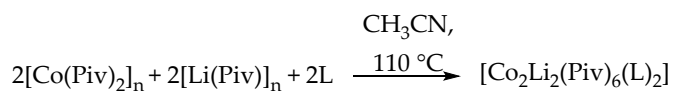
1.2 Synthesis of 4-MeOC₆H₄-MIAN

A solution of 27.47 mmol (5 g) acenaphthenequinone and 27.47 mmol (3.78 g) of *p*-anisidine in 120 ml of toluene and 0.5 mL acetic acid was refluxed 1h using reflux condenser and then also 1h with Dean-Stark apparatus for water separation. The toluene was removed and the solid residue was redissolved in acetone. Upon slow evaporation of the solution, the crystalline red product (4-MeOC₆H₄-MIAN) was isolated by decantation and dried at ambient conditions (6.78 g, yield 86%).

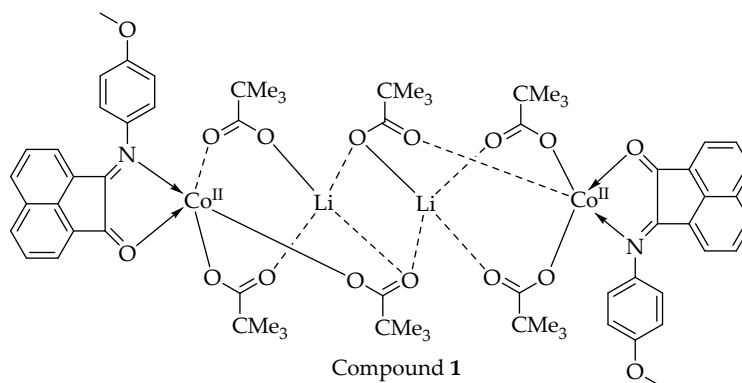
Anal. calcd for C₁₉H₁₃NO₂ (287.31) C, 79.43; H, 4.56; N, 4.88. Found: C, 79.03; H, 4.75; N, 4.63. IR, v/cm⁻¹: 1653 w, 1620 m, 1603 s, 1582 m, 1508 vs, 1421 w, 1302 s, 1287 m, 1252 vs, 1183 w, 1172 s, 1150 w, 1123 m, 1069 m, 1052 w, 1028 s, 959 w, 936 w, 920 w, 869 m, 837 s, 832 s, 814 w, 806 m, 782 s, 735 m, 658 m, 642 w, 604 m, 542 s, 524 w, 497 s. NMR ¹H (CDCl₃, 27°C, δ/ppm): 8.18-8.12 (m, 2H), 7.99 (d, 1H), 7.78 (t, 1H), 7.45 (t, 1H), 7.25 (d, 1H), 7.10 (d, 2H), 7.00 (d, 2H), 3.88 (s, 3H).

1.3 Synthesis of [Co₂Li₂(Piv)₆(4-MeOC₆H₄-MIAN)₂]·CH₃CN (**1**)

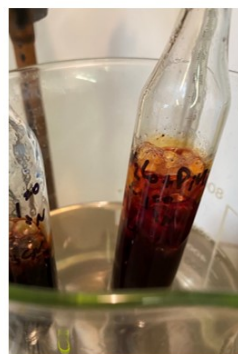
Weighed portions of [Co(Piv)₂]_n (0.260 g, 1.000 mmol), [Li(Piv)]_n (0.108 g, 1.000 mmol) and 4-MeOC₆H₄-MIAN (0.287 g, 1.000 mmol) were placed in a thick-walled glass ampoule (V = 30 ml) and degassed in a dynamic vacuum with a cold trap for 20 min, dry acetonitrile was condensed into the ampoule, the latter was fire-sealed and heated in an oil bath (110 °C, *caution – high pressure!*) for 15 h until the all initial reagents dissolved. The reaction mixture color changed from purple to the red one. Brown crystals of the product were grown with further cooling an oil bath to room temperature and isolated by decantation, twice washed with cold acetonitrile (0.548 g, 81 %). Anal. calcd for C₇₀H₈₃Co₂Li₂N₃O₁₆ (1354.16) C, 62.09; H, 6.18; N, 3.10. Found: C, 61.94; H, 6.02; N, 3.01. IR, v/cm⁻¹: 2955 m, 2929 w, 2868 w, 2834 w, 1715 w, 1603 s, 1586 m, 1557 s, 1527 m, 1499 m, 1487 s, 1408 s, 1356 m, 1284 m, 1229 vs, 1172 w, 1095 w, 1030 m, 928 w, 903 w, 831 w, 775 m, 749 w, 719 w, 603 m, 573 w, 535 w, 435 m, 408 vs.



1 (81%)

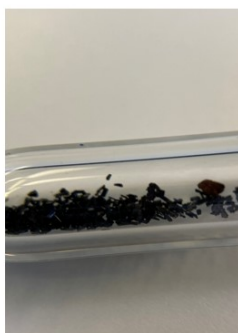
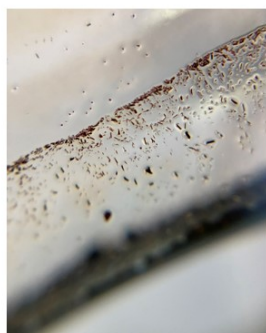


Scheme S1. Synthesis of complex **1**.



Weighed portions of [Co(Piv)₂]_n (0.260 g, 1.000 mmol), [LiPiv]_n (0.108 g, 1.000 mmol) and 4-MeOC₆H₄-MIAN (0.287 g, 1.000 mmol) were placed in a thick-walled glass ampoule (V = 30 ml) and degassed in a dynamic vacuum with a cold trap for 20 min, dry acetonitrile was condensed into the ampoule

The latter was fire-sealed and heated in an oil bath (110° C, caution – high pressure!) for 15 h until the all initial reagents dissolved



Brown crystals of the product were grown with further cooling an oil bath to RT and isolated by decantation, twice washed with cold acetonitrile

Isolated single crystals in a sealed glass ampoules

Figure S1. Synthesis of [Co₂Li₂(Piv)₆(4-MeOC₆H₄-MIAN)₂]-CH₃CN (**1**)

2. NMR spectroscopy

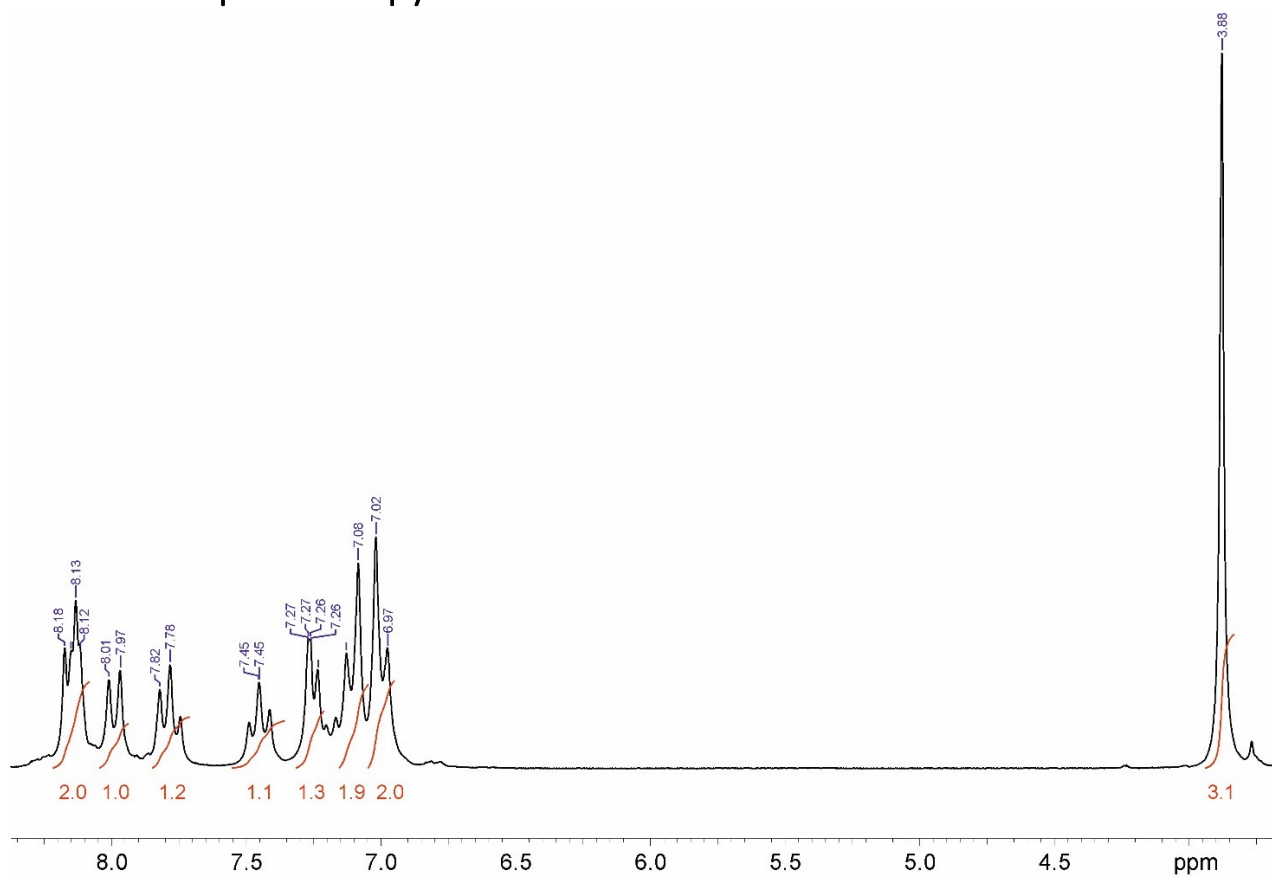


Figure S2. ^1H NMR of 4-MeOC₆H₄-MIAN in CDCl₃.

3. IR spectroscopy

IR spectra were recorded in the range 400–4000 cm^{-1} on a Perkin Elmer Spectrum 65 spectrophotometer equipped with Quest ATR Accessory (Specac) using the method of attenuated total reflection (ATR).

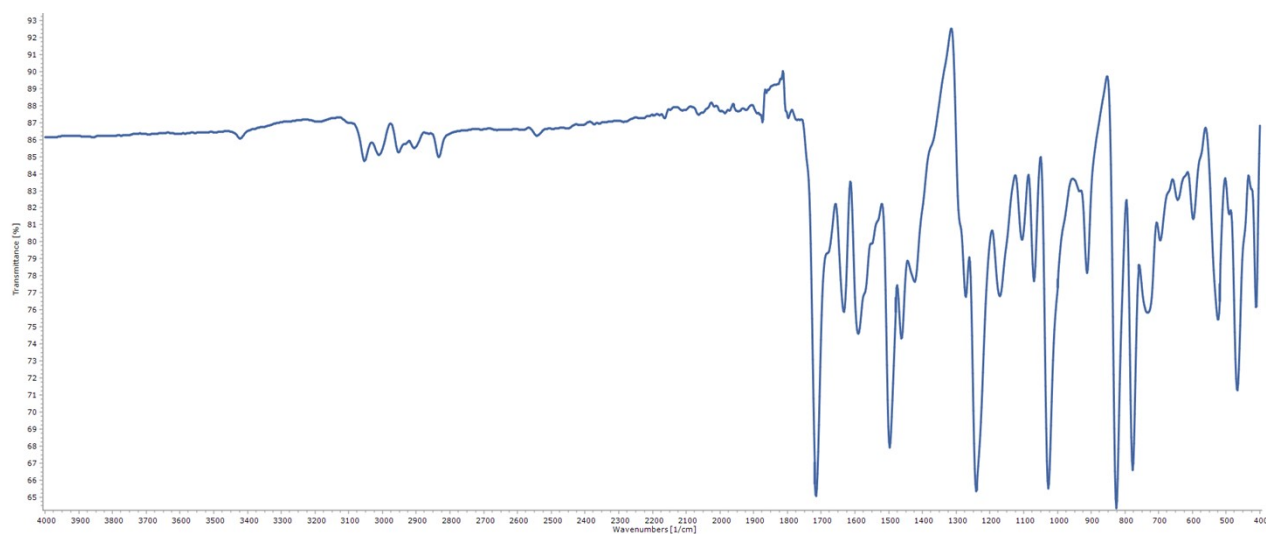


Figure S3. IR spectrum of 4-MeOC₆H₄-MIAN

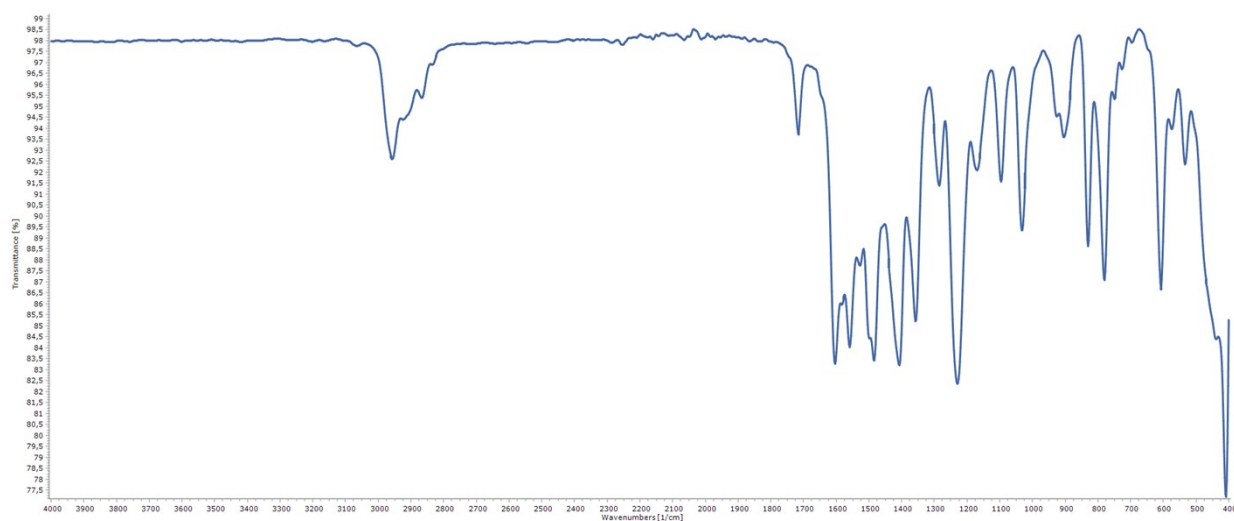


Figure S4. IR spectrum of **1**.

4. Single crystal X-ray diffraction

The X-ray diffraction data for the crystal **1** were collected at 296K on a Bruker SMART Apex II diffractometer equipped with a CCD detector (Mo-K α , $\lambda = 0.71073$ Å, graphite monochromator). Semi-empirical absorption correction was applied by the SADABS program [S4]. The structure was solved by direct methods and refined by the full-matrix least squares in the anisotropic approximation for non-hydrogen atoms. The calculations were carried out by the SHELX-2014 program package [S5] using Olex2 1.2 [S6]. Crystallographic data for **1** reported in this paper have been deposited with the Cambridge Crystallographic Data Center (2221163). Crystal data for **1**: C₆₈H₈₀Co₂Li₂N₂O₁₆·C₂H₃N, $M = 1354.13$ g mol⁻¹, colorless crystal, monoclinic, space group $P2_1$, $Z = 2$, $a = 11.6202(11)$, $b = 19.455(2)$, $c = 16.1507(18)$ Å, $\beta = 101.367(4)^\circ$, $V = 3579.6(7)$ Å³, $\rho_{\text{calc}} = 1.256$ g cm⁻³, $\mu = 0.53$ mm⁻¹, 46003 reflections collected (h, k, l), 12260 independent ($R_{\text{int}} = 0.150$) and 6545 observed reflections [$I > 2\sigma(I)$], 868 refined parameters, $R_1 = 0.0878$, $wR_2 = 0.2321$, max. residual electron density is 0.94 (-0.60) eÅ⁻³.

Table S1. Selected bond lengths and angles in the molecule of **1** in the crystal.

Bond	Bond length, Å	Bond	Bond length, Å
O7-C46	1.224(17)	O14-C58	1.218(16)
N1-C45	1.284(16)	N2-C57	1.276(16)
C45-C46	1.49(2)	C57-C58	1.531(19)
O2-Li1	1.97(3)	Co1-O1	1.978(9)
O2-Li2	1.93(2)	Co1-O3	1.993(11)
O4-Li1	1.90(3)	Co1-O5	2.077(11)
O6-Li1	1.90(3)	Co1-O6	2.190(10)
O9-Li1	1.94(2)	Co1-O7	2.343(10)
O9-Li2	1.98(2)	Co1-N1	2.145(12)
O11-Li2	1.87(2)	Co2-O8	2.000(9)
O13-Li2	1.87(2)	Co2-O10	1.993(10)
Co2-O14	2.276(10)	Co2-O12	2.077(10)
Co2-N2	2.139(11)	Co2-O13	2.173(9)
Angle	Angle, °	Angle	Angle, °
O1-Co1-O3	102.3(4)	O8-Co2-O12	95.3(4)
O1-Co1-O5	96.0(4)	O8-Co2-O13	95.9(3)
O1-Co1-O6	94.7(4)	O8-Co2-O14	173.6(4)
O1-Co1-O7	167.5(4)	O8-Co2-N2	96.4(4)
O1-Co1-N1	91.2(4)	O10-Co2-O8	102.9(4)
O3-Co1-O5	157.1(4)	O10-Co2-O12	158.0(4)
O3-Co1-O6	102.9(4)	O10-Co2-O13	103.8(4)
O3-Co1-O7	79.1(4)	O10-Co2-O14	80.0(4)
O3-Co1-N1	88.3(4)	O10-Co2-N2	88.4(4)
O5-Co1-O6	61.5(4)	O12-Co2-O13	61.6(3)
O5-Co1-O7	86.1(4)	O12-Co2-O14	83.2(3)
O5-Co1-N1	105.1(4)	O12-Co2-N2	101.9(4)
O6-Co1-O7	97.1(3)	O13-Co2-O14	88.8(3)
N1-Co1-O6	165.9(4)	N2-Co2-O13	160.3(4)
N1-Co1-O7	76.4(4)	N2-Co2-O14	78.0(4)

There are no hydrogen binding centers in the molecule of **1**. The main structure-forming motif is the formation of infinite chains due to the π -stacking interactions between polycyclic aromatic ligand fragments (Fig. S5, Table S2). The chains are located almost perpendicular to each other due to the translation along axis 2_1 and are connected to a three-dimensional grid by weak CH...O (C...O distances are 2.8-3.4 Å) and CH... π (C... centroid of the ring distances are 3.7-3.9 Å) interactions.

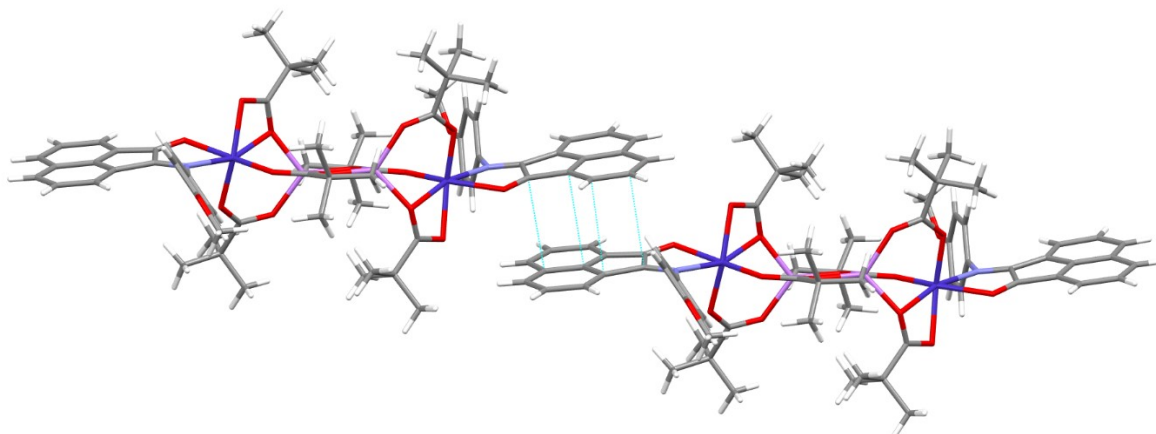


Figure S5. Intermolecular π ... π interactions in the crystal of **1**.

Table S2. π ... π interactions in the crystal of compound **1**.

Interaction	Symmetry generation	Cg-Cg, Å	Alpha,°	Beta,°	Gamma,°	CgI_Perp, Å	CgJ_Perp, Å	Slippage, Å
Cg4...Cg10*	1+x,y,1+z	3.424(8)	3.8(8)	9.6	7.8	3.393(6)	3.376(6)	0.570
Cg5...Cg8	-1+x,y,-1+z	3.497(8)	1.9(7)	12.9	14.7	3.383(6)	3.408(6)	0.778
Cg8...Cg10	1+x,y,1+z	3.898(9)	1.6(7)	28.2	29.0	3.410(6)	3.435(6)	1.842

*Cg is centroid of rings (Cg4 - C45-C46-C47-C56-C55; Cg5 - C57-C58-C59-C68-C67; Cg8 - C47-C48-C49-C50-C51-C56; Cg10 - C59-C60-C61-C62-C63-C68).

5. Powder X-ray diffraction studies

The powder patterns were measured on a Bruker D8 Advance diffractometer with LynxEye detector in Bragg-Brentano geometry, with the sample dispersed thinly on a zero-background Si sample holder, $\lambda(\text{CuK}\alpha) = 1.54060 \text{ \AA}$, θ/θ scan with variable slits (irradiated length 20 mm) from 5° to $45^\circ 2\theta$, stepsize 0.02° . The obtained patterns were Rietveld refined using TOPAS 4 software (Fig. S6).

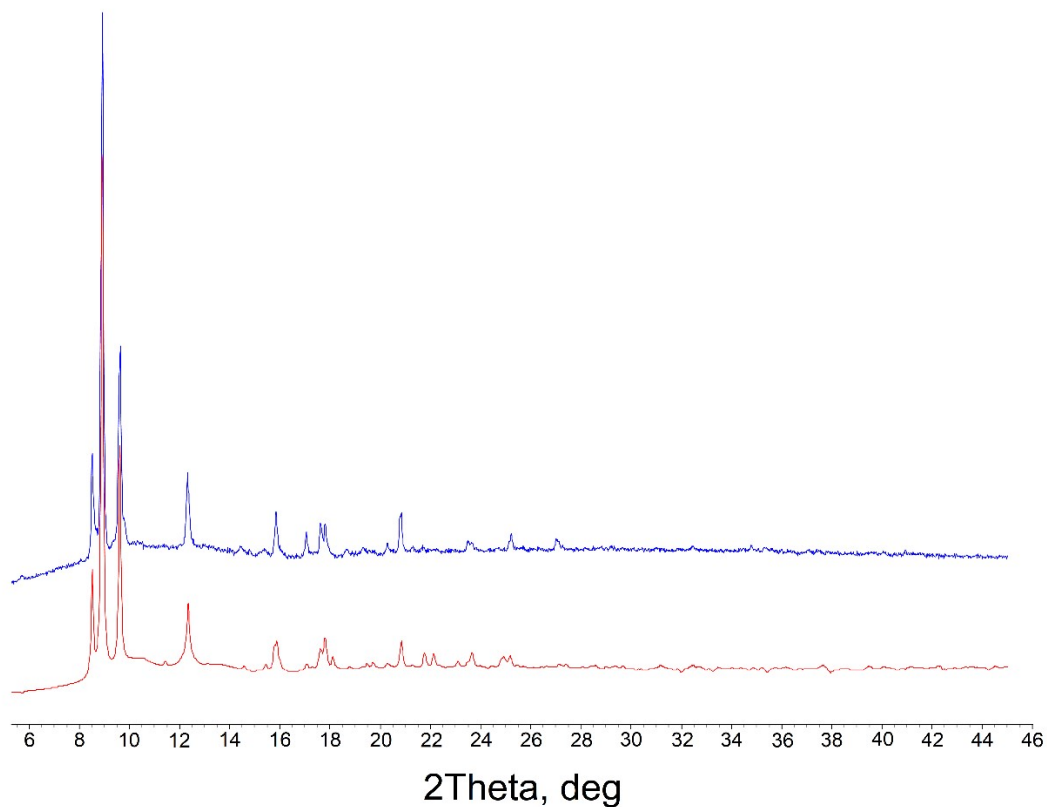


Figure S6. Theoretical (red) and experimental (blue) X-ray powder diffraction patterns of sample **1**.

6. Magnetochemistry

Magnetic susceptibility measurements were performed with a Quantum Design susceptometer PPMS-9. The temperature dependences of the magnetization (M) were measured in 1000 and 5000 Oe magnetic fields in the temperature range 2–300 K during cooling at a cooling rate of 1 K/min. During ac -susceptibility measurements in the frequency range of 10–10⁵ Hz, an alternating magnetic field amplitude was $H_{ac} = 1–5$ Oe. The measurements were carried out for the samples moistened with mineral oil to prevent any texturizing of the particles in dc -magnetic field. The prepared samples were sealed in polyethylene bags. The paramagnetic components of the magnetic susceptibility χ were determined taking into account the diamagnetic contribution evaluated from Pascal's constants as well as the contributions of the sample holder and mineral oil. The dc -magnetic data were fitted using the PHI program [S7].

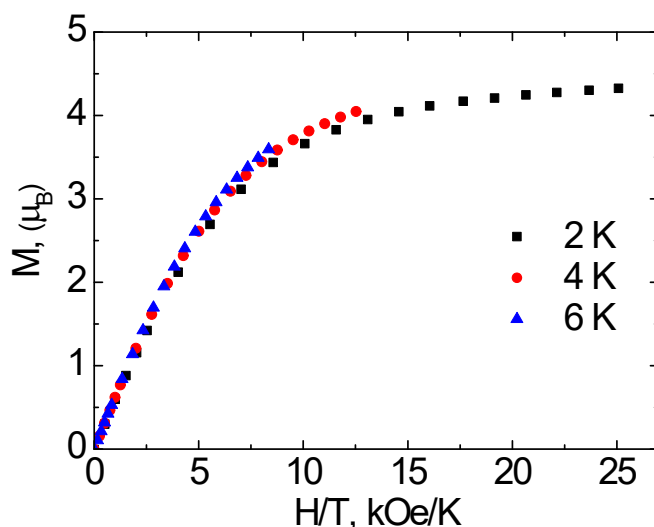


Figure S7. The $M(H/T)$ dependences at different temperatures for compound **1**.

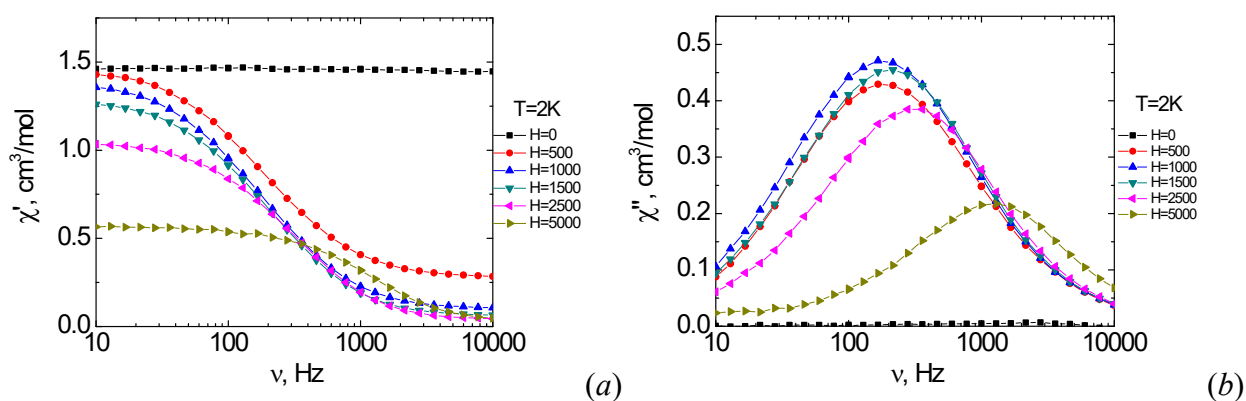


Figure S8. Frequency dependences of the real (χ' , *a*) and imaginary (χ'' , *b*) components of the ac susceptibility under at 2 K for **1** in various dc -fields. Solid lines are visual guides (χ' , *a*) and represent fitting by generalized Debye model (χ'' , *b*).

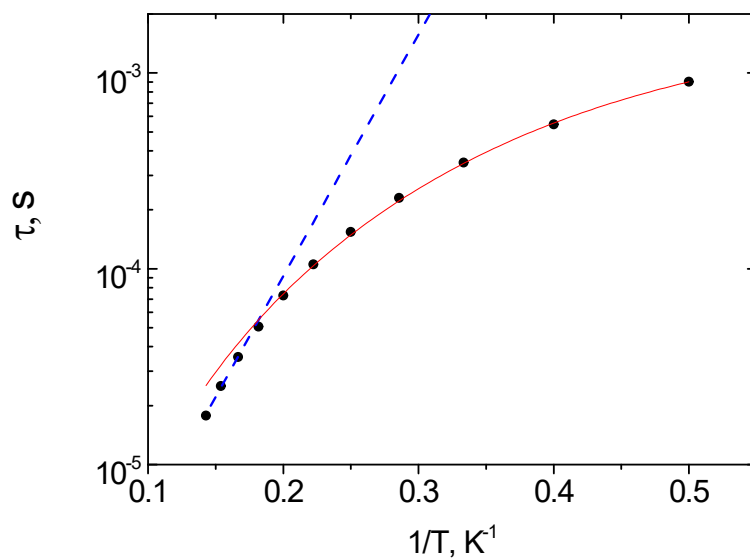


Figure S9. τ vs. T^{-1} plot for **1** in 1000 Oe dc -field. Blue dashed line represents the best fit by the Orbach mechanism (Arrhenius equation) in high temperature range. Red solid line represents the best fit by the sum of the **Raman + QTM** relaxation mechanisms in whole temperature range.

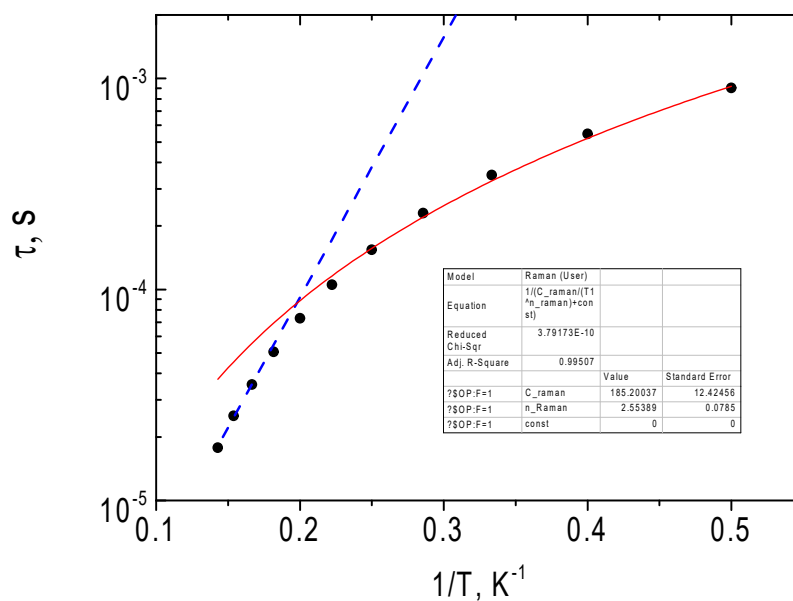


Figure S10. τ vs. T^{-1} plot for **1** in 1000 Oe dc -field. Blue dashed line represents the best fit by the Orbach mechanism (Arrhenius equation) in high temperature range. Red solid line represents the best fit by the **Raman** relaxation mechanism in whole temperature range.

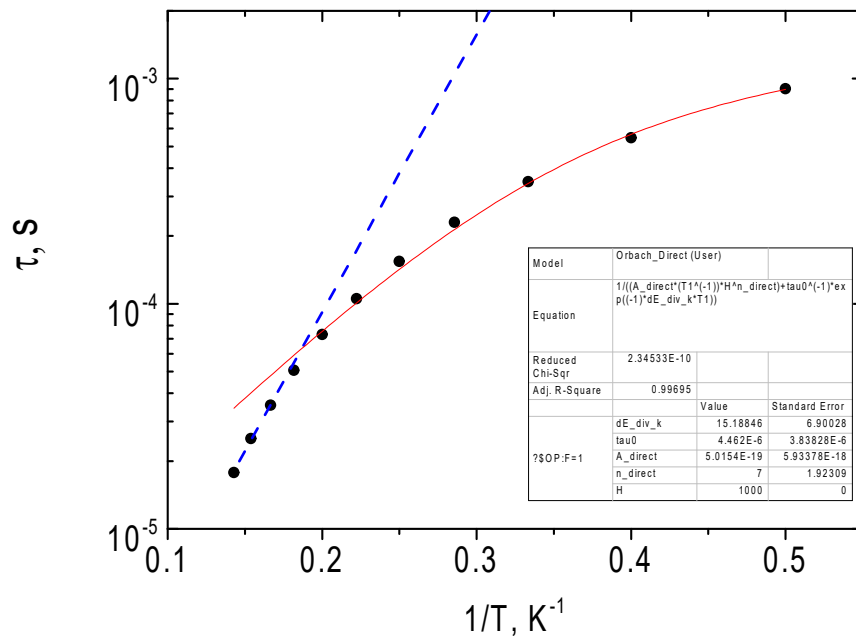


Figure S11. τ vs. T^{-1} plot for **1** in 1000 Oe dc -field. Blue dashed line represents the best fit by the Orbach mechanism (Arrhenius equation) in high temperature range. Red solid line represents the best fit by the sum of the **Orbach + direct** relaxation mechanisms in whole temperature range.

7. Quantum-chemical calculations

Ab initio (post Hartree–Fock) calculations of ZFS parameters and *g*-tensor were performed based on state-averaged complete-active-space self-consistent-field (SA-CASSCF) wave function [S8] complemented by N-electron valence second-order perturbation theory (NEVPT2) [S9] using the ORCA program package (version 5.0.1) [S10]. The calculations were performed with the geometry of the experimentally determined X-ray structures. The active space of the CASSCF calculations was composed of seven electrons in five d-orbitals of Co²⁺ ions (*S* = 3/2): CAS(7,5). The state-averaged approach was used, in which all 10 quartet (*S* = 3/2) and 40 doublet (*S* = 1/2) states were averaged with equal weights. The polarized triple- ζ -quality basis set def2-TZVP was used for all atoms [S11]. An auxiliary def2/JK Coulomb fitting basis set was used during the calculation [S12]. Both the zero-field splitting parameter (*D*) and transverse anisotropy (*E*), based on dominant spin-orbit coupling contributions from excited states, were calculated through quasi-degenerate perturbation theory (QDPT) [S13], where approximation to the Breit-Pauli form of the spin-orbit coupling operator (SOMF) [S14] and an effective Hamiltonian approach [S15]. The splitting of the d-orbitals was analyzed within the *ab initio* ligand field theory (AILFT) [S16, S17]. The AILFT d-orbitals are described as their linear combinations. Splitting is presented based on the largest coefficients for each orbital. The parameters of symmetry distortion of polyhedra from ideal point groups were calculated using the program ChemCraft [S18].

Table S3. Coefficients of symmetry distortion from the ideal polyhedron for Co1 and Co2 atoms.

Coordination environment	Co1 ²⁺	Co2 ²⁺
Coordination number 5		
vOC (C _{4v})	2.59	2.47
SPY (C _{4v})	3.16	2.52
TBPY (D _{3h})	6.38	6.85
Coordination number 6		
OC (O _h)	2.83	2.28
TPR (D _{3h})	12.82	14.86

vOC – vacant octahedron, SPY – square pyramid, TBPY – trigonal bipyramid, OC – octahedron, TPR – trigonal prism.

Table S4. CASSCF/NEVPT2 calculated ground and spin-orbit states of individual Co1²⁺ and Co2²⁺ ions (cm⁻¹).

	Co1 ²⁺	Co2 ²⁺
⁴ A ₂	0	0
⁴ E	1704.7	1561.5
	2388.1	2355.4
	0	0
KDs	101.3 δ	108.8 δ
	1738.0	1614.1
	1928.7	1805.3
	2545.3	2518.6
	2643.8	2612.5
ζ	524.41	524.44

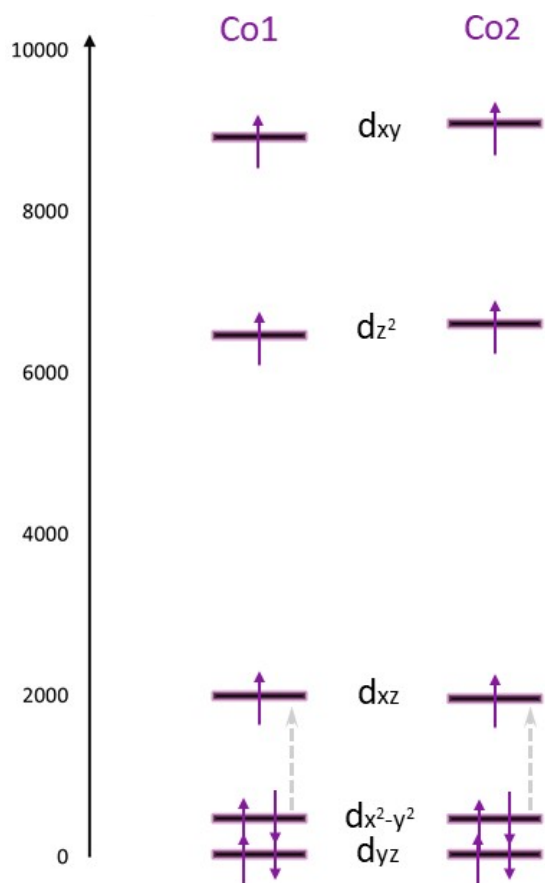
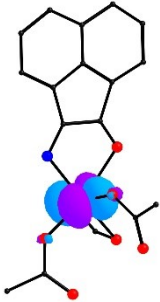
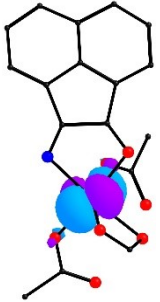
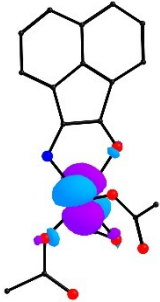
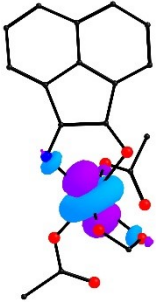
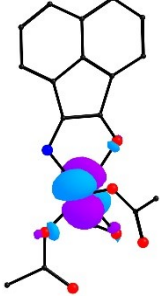
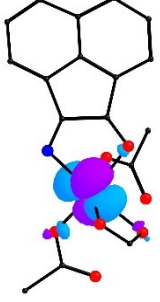
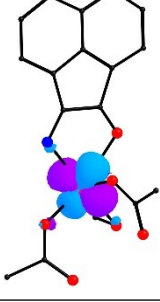
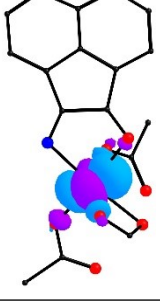
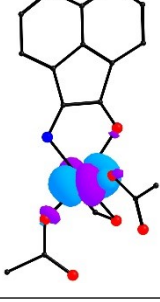
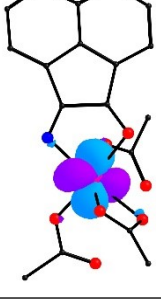


Figure S12. Relative energies of d-orbitals splitting of $Co1^{2+}$ and $Co2^{2+}$ ions in C_{4v} crystal field according to *AILFT*. The grey dashed lines mark the energy difference.

Table S5. Relative energies of d-AO splitting of Co1²⁺ and Co2²⁺ ions according *AIFLT*. Substituents at the ligands are partially hidden for clarity. Contour value is 0.036 e/Å³.

d-orbitals	Co1 ²⁺		Co2 ²⁺	
dxy		8873.8 cm ⁻¹		9041.0 cm ⁻¹
dz ²		6424.4 cm ⁻¹		6563.7 cm ⁻¹
dxz		1957.4 cm ⁻¹		1922.4 cm ⁻¹
dx ² -y ²		444.2 cm ⁻¹		435.4 cm ⁻¹
dyz		0 cm ⁻¹		0 cm ⁻¹

8. References

- S1. I.G. Fomina, G.G. Aleksandrov, Zh.V. Dobrokhotova, O.Yu. Proshenkina, M.A. Kiskin, Yu.A. Velikodnyi, V.N. Ikorskii, V.M. Novotortsev and I.L. Eremenko, *Russ. Chem. Bull.*, 2006, **55**, 1909, doi:10.1007/s11172-006-0532-4.
- S2. E.N. Zorina-Tikhonova, D.S. Yambulatov, M.A. Kiskin, E.S. Bazhina, S.A. Nikolaevskii, N.V. Gogoleva, I.A. Lutsenko, A.A. Sidorov and I.L. Eremenko, *Russ. J. Coord. Chem.*, 2020, **46**, 75, doi:10.1134/S1070328420020104.
- S3. I. Mhaidat, S. Hamilakis, C. Kollia, A. Tsolomitis and Z. Loizos, *Mater. Lett.*, 2006, **60**, 147, doi:10.1016/j.matlet.2005.07.032.
- S4. G.M. Sheldrick, SADABS. Madison (WI, USA): Bruker AXS Inc.; 1997.
- S5. G.M. Sheldrick, *Acta Crystallogr. Sect. A*, 2015, **71**, 3, doi:10.1107/S2053273314026370.
- S6. O.V. Dolomanov, L.J. Bourhis, R.J. Gildea, J.A.K. Howard and H. Puschmann, *J. Appl. Crystallogr.*, 2009, **42**, 339, doi:10.1107/S0021889808042726.
- S7. N.F. Chilton, R.P. Anderson, L.D. Turner, A. Soncini, K.S. Murray, *J. Comput. Chem.*, 2013, **34**, 1164, doi:10.1002/jcc.23234.
- S8. P.-Å. Malmqvist and B.O. Roos, *Chem. Phys. Lett.*, 1989, **155**, 189, doi:10.1016/0009-2614(89)85347-3.
- S9. C. Angeli, R. Cimiraglia, S. Evangelisti, T. Leininger and J.-P. Malrieu, *J. Chem. Phys.*, 2001, **114**, 10252, doi:10.1063/1.1361246.
- S10. F. Neese, *WIREs Comput. Mol. Sci.*, 2012, **2**, 73, doi:10.1002/wcms.81.
- S11. A. Schäfer, C. Huber and R. Ahlrichs, *J. Chem. Phys.*, 1994, **100**, 5829, doi:10.1063/1.467146.
- S12. F. Neese, *J. Comput. Chem.*, 2003, **24**, 1740, doi:10.1002/jcc.10318.
- S13. D. Ganyushin and F. Neese, *J. Chem. Phys.*, 2006, **125**, 24103, doi:10.1063/1.2213976.
- S14. F. Neese, *J. Chem. Phys.*, 2005, **122**, 34107, doi:10.1063/1.1829047.
- S15. R. Maurice, R. Bastardis, C. de Graaf, N. Suaud, T. Mallah and N. Guihéry, *J. Chem. Theory Comput.*, 2009, **5**, 2977, doi:10.1021/ct900326e.
- S16. S.K. Singh, J. Eng, M. Atanasov and F. Neese, *Coord. Chem. Rev.*, 2017, **344**, 2, doi:10.1016/j.ccr.2017.03.018.
- S17. D.M.P. Mingos, P. Day and J.P. Dahl (Eds), *Molecular Electronic Structures of Transition Metal Complexes II (Structure and Bonding, Book 143)*; Springer, 2012; ISBN 3642273777.
- S18. ChemCraft Version 1.8, build 648; <https://www.chemcraftprog.com>